Resonant Raman Scattering in Undoped and Lanthanide-Doped CeO2

Resonant Raman Scattering in Undoped and Lanthanide-Doped CeO_2

Olga Kraynis[1], Igor Lubomirsky[1] and Tsachi Livneh[2]*

[1]Dept. Materials and Interfaces, Weizmann Institute of Science, Rehovot 76100, Israel
[2] Dept. Physics, Nuclear Research Center Negev, P.O. box 9001, Beer Sheva 84190, Israel

Abstract

CeO_2 has a narrow, empty band of *Ce4f* states that lies between a *O2p* based valence band and a *Ce5d* based conduction band. The *O2p* - *Ce4f* optical band gap is positioned at ~3.2 eV with an absorption band centered at ~3.8 eV. We investigated the Raman scattering of bulk CeO_2 in the excitation energy range of 1.96–3.81 eV. The resonant enhancement profile of the longitudinal optical (LO) phonon at ~590 cm^{-1}, closely follows that of the 2LO band and both profiles track the optical absorption of the O*2p* - Ce*4f* electronic transition. Multi-LO phonon bands were found to appear up to the sixth-order, pointing to an electron-phonon Fröhlich interaction as the source of the resonant enhancement. The ~600 cm^{-1} off-resonant D_2 band (denoted as MO_8-type complex in ceria doped with M aliovalent ions), is overshadowed under resonant conditions by the resonant LO phonon scattering. Hence, spectral analysis of defect bands under resonant conditions has to be distinct from that applied under off-resonant conditions and care must be taken when dealt-with under a single framework.

We investigated the resonant Raman spectra of Lu, La, Gd or Sm-doped ceria ceramic pellets as a function of increasing Do^{3+} *mol*%, in the Fluorite phase range (up to 20mol%). For La and Lu the general trend of the Do^{3+} *mol*% frequency dependence for the D_1 *local mode* is qualitatively similar to that of the F_{2g} *phonon* and it follows the respective expansion (La) or contraction (Lu) in the lattice parameter. However, for Gd and Sm, the trend is opposite to the F_{2g} mode. This trend may stem from local lattice contraction around point defects, which was suggested, based on local structure probes such as X-ray absorption spectroscopy and pair distribution function analysis of X-ray diffraction. Our analysis provides access to average as well as to local structures of ceria solid solutions, *via* Resonant Raman spectroscopy.

1 Introduction

Raman scattering is widely used in characterizing ceria and aliovalent cation doped ceria (mostly trivalent lanthanides, Do^{3+}) [1-7]. The majority of Raman studies are using off-resonant laser excitations far below the band gap. However, since shorter wavelengths in ceria provide smaller penetration depths, UV (>3.4 eV) Raman has emerged as a suggested tool to characterize the structure of defect sites at the near-surface (up to few tenths of nm) area of ceria and doped ceria [3-5].Those defects sites play a key role in catalytic processes.

CeO_2 has a narrow, empty band of *Ce4f* states that lies between a *O2p* based valence band and a *Ce5d* based conduction band. The *O2p - Ce4f* optical band gap is positioned at ~3.2 eV with an absorption band centered at ~3.8 eV [8]. The excitation energy used for UV- Raman studies is therefore sufficient to enter the Resonant Raman regime. This introduces additional spectral contributions to the ceria Raman spectrum and most importantly the ceria Raman defect spectrum. When analyzing the defect structure under UV excitation, resonance related effects must therefore be considered alongside with effects resulting from the decrease in penetration depth.

To understand these contributions, we first describe the current assignment of the undoped and doped ceria spectrum under off-resonant and resonant conditions. Weber et al. [1] explored the *off-resonant* polarized Raman scattering of undoped single crystal of ceria. The spectra contained contributions from an F_{2g} symmetry band at 465 cm^{-1}; a series of second-order bands of Brillouin zone (BZ) edge phonons and an overtone of the longitudinal optic (2LO) band at ~1180 cm^{-1}. In a Fluorite structure, the LO phonon, expected at ~592 cm^{-1} [9], is Raman forbidden by symmetry (F_{1u}), unlike the 2LO band, which contains the symmetric A_{1g} representation and therefore is allowed [1]. Nakajima et al. [2] explored the spectral manifestations of defect structures, introduced when the Ce^{4+} host is replaced by an aliovalent dopant, also under off-resonant conditions. In the 500-600 cm^{-1} range they suggested a defect scheme consisting of two bands. (i) A lower band (D_1) at ~540 cm^{-1}, attributed to two types of oxygen vacancies (V_O), formed as a charge balance when Ce^{4+} ions are substituted by Ce^{3+} in reduced CeO_2, or by Do^{3+} ions in doped ceria. (ii) D_2-band at ~600 cm^{-1}, which was attributed to a dopant cation in 8-fold coordination of O^{2-}, denoted as MO_8-type complex (M in this case is Do^{3+}). We also note that in a recent report that includes a detailed DFT analysis of undoped bulk ceria [7] it was argued that the spectral region of the D_1 band can be assigned to the $Ce^{4+}O_7V_O$ coordination, whereas the D_2 region is attributed to the $Ce^{3+}O_7V_O$ (i.e., Ce^{3+} reduction

close to a defect) coordination cube. Nevertheless, since the assignment of the D_1 and D_2 [2] is commonly used in the literature, it will also be used here, while noting that such attribution may deserve scrutiny.

In an ideal crystal structure, the momentum (wave-vector) conservation restricts the first-order Raman scattering to lattice vibrations from the center of the BZ (**k**~0). Since phonons with F_{1u} symmetry are not Raman-allowed, the LO phonon is not expected in the off-resonant Raman spectrum of an ideal CeO_2 crystal. Due to the long-range interactions generated by the macroscopic electric-field associated with an LO phonon, it may, however, be resonantly activated when the frequency of the incident light approaches a characteristic electronic transition. In such a scenario, commonly attributed to the Fröhlich electron-phonon interactions [9], a *complete* set of 1LO to multi-phonon manifold may emerge in the *resonant* Raman spectrum. Once activated, the LO phonon is expected to overlap with the aforementioned D_2 defect band.

Taniguchi et al. [3] explored the Raman scattering of undoped and Gd-doped (up to 20 mol%) ceria with above-bandgap UV laser energy of 3.41 eV and found enhanced intensities of the overtone bands of 2LO (~1170 cm^{-1}) and 3LO (~1750 cm^{-1}). The bands at 500-600 cm^{-1} were also found to have enhanced intensities and were assigned to the D_1 and D_2 bands, in accordance with the off-resonant assignment [2]. A later UV-resonant study [5] used this assignment as a qualitative tool to assess the relative abundance of D_1 and D_2 type defects for various Lanthanide-doped ceria and the effect of heat treatment on their ratio. The intensity enhancement of the defect bands in the UV-Raman spectrum were attributed to the small (few tenths of nm) penetration depth and to their relative abundance at the near-surface area.

A major drawback in those UV-Raman studies [3, 5] is that the resonant nature of the scattering process (which was manifested in the intensities of the second-forth order LO phonon scattering) was discussed while disregarding the participation in the Raman spectrum of the first-order Raman LO phonon. In the case of CeO_2 this drawback is particularly stringent due to the ~8 cm^{-1} proximity in frequencies of the D_2 local defect mode and the LO phonon, which may result in erroneous quantitative analysis of the near-surface defect scheme under resonant conditions.

It is evident from recent studies that the dopant fraction (Do^{3+} mol%) dependence of the *local* interatomic distances in Lanthanide-doped ceria, as extracted from X-ray absorption fine

structure (EXAFS)[10-13] as well as X-ray diffraction (XRD) based pair distribution function (PDF) analysis [14, 15], may significantly differ from that of the interatomic distances, extracted from *average* structure measured by Rietveld or conventional XRD refinement. A short literature summary of these trends for several dopants with ascending Shannon ionic radii (Coordination VIII) Lu (97.7pm) < Gd (105pm) < Sm (108pm) < La (116pm), is given in the SI **Figure S1**. The literature data reveals that, while similar trends in *Average* and *local* structures are found for the dopants at the two extremes of Shannon ionic radii (La and Lu), opposite trends in *average vs*. *local* structures are found for Gd and Sm-doped ceria. Namely, the lattice parameter for Gd and Sm expands with increasing Do^{3+} mol%, while first shell local distances around the cation species, *Ce-O* and *Do-O*, contract. This unique structural behavior may also be linked to the fact these dopants exhibit large ionic conductivities[16]. These clear discrepancies between local and average environment, which also support the existence of local strain (at first and second coordination shells of a lattice site)[10] are suggested to be the microscopic source of the anelastic and electro-mechanic effects observed in these materials [17]. Furthermore, the contraction observed in the first shell distances *Ce-O* and *Do-O* by EXAFS is likely occurring in the vicinity of V_O defects. In their *off-resonant* Raman study, Artini et al.[6] demonstrated for an increasing Do^{3+} mol% of Sm doped ceria that the F_{2g} mode and the defect area in the 500-600 cm^{-1} range follow separate trends for different ranges of doping. These observations indicate that the deviation of *average* and *local* structural trends may be identified *via* Raman scattering measurements.

In the current study we first elucidate the nature of resonant UV-Raman scattering in CeO_2 and discuss the implications of the resonant emergence of the LO phonon on the spectral analysis of defect bands at 500-600 cm^{-1} range, which is extensively referred-to in the literature. We then use our assignment of the defect bands under the defect sensitive UV-Raman regime in order to study the Do^{3+} composition dependence of the various mode frequencies in the resonant Raman spectra of Lu, La, Gd and Sm-doped ceria ceramic pellets. We focus on the technologically important Fluorite phase where Do^{3+} fraction is < 20 mol%. Our objective is to provide supporting evidence from the Raman spectra to the deviation of *local* and *average* structures, in Gd and Sm-doped ceria as demonstrated from the comparison of XRD and synchrotron- based techniques.

2 Experimental

Raman spectra were collected in the back-scattering configuration with two Horiba LabRAM HR Evolution micro-Raman spectrometers with 1800 lines/mm grating using the excitation laser energies (wavelengths) of He-Ne laser 1.96 eV (632.8 nm), diode lasers of 2.33 eV (532 nm), 3.06 eV (405 nm) and He-Cd laser of 3.81 eV (325 nm). The spectra were acquired from: i. An undoped ceria pellet. ii. A series of doped ceria materials $Ce_{1-x}Do_xO_{2-x/2}$ (Do = Lu, Gd, Sm, La with varying doping fraction *x* within the XRD Fluorite phase), as well as from iii. A 4mol% Sm - doped ceria thin film. The undoped ceria pellet, Gd and Lu doped materials have average grain size of 1.6 μm, an estimated O vacancy concentration of <1% and were prepared by the co-precipitation method, calcined, pressed and sintered at 1300ºC, as described by Yavo et al.[18]. XRD data for Gd doped solid solutions is available in reference [19], while XRD data for Lu solid solutions are provided in the SI of reference [20]. The grain sizes for Sm and La-doped materials were 10-25μm. Sm solid solutions were synthesized using solid state reactions as described in references [21, 22]. XRD data for the materials is available in the supplementary data of reference [21]. La solid solutions were synthesized using co-precipitation method, calcined pressed and sintered to 1500ºC, as described in reference [23]. The 4% Sm-doped ceria thin film with thickness of ~1μm, and columnar grain structure of ~20 nm lateral dimension, was prepared by magnetron sputter deposition (AJA®) as described in supporting information (see XRD pattern in SI **Figure S2)**.

3 Results and discussion

3.1. The resonant nature of the LO mode and its overshadowing of the D_2 defect mode

Raman spectra collected from the undoped CeO_2 pellet, at excitation energies of 2.33, 3.06 eV (*off-resonance*) and 3.81 eV (*under resonance*) are shown in **Figure 1a**. The 3.81 eV spectrum mainly consists of the Raman-allowed F_{2g} mode at 464 cm^{-1}, a feature around 500- 600 cm^{-1} that contains two bands, centered at ~543cm^{-1} and ~590 cm^{-1}, and bands of higher order LO phonons: 2LO, 3LO and 4LO bands centered at ~1172, ~1754 and ~2352 cm^{-1}, respectively (see **Figure S3** of the SI for an extended spectral range). In addition, a weak fifth (~2940 cm^{-1}) and possibly sixth-order LO modes are resolved. In **Figure 1b** the appearance of LO modes is demonstrated by "slicing" the spectra into segments that are shifted by $-n\cdot\omega_{LO}$ from the original spectrum with ω_{LO}=586 cm^{-1} of the n-order band.

In order to determine whether the ~590cm^{-1} band is enhanced under resonance, we plot the normalized (to the F_{2g} mode) intensities of the 2LO and ~590 cm^{-1} bands, against the excitation energy (E_i). We than compare them to the excitation energy dependence of the absorption coefficient, α, which is derived from the extinction coefficient, ε_2, of bulk CeO_2 [8] (see **Figure 2**) according to $\alpha=4\pi\varepsilon_2/\lambda$ (with λ- the excitation wavelength). In addition to the intensity ratios derived from the spectra measured in this study, we show the normalized intensities of the above two bands, extracted from previously published spectra measured at E_i of 3.41eV and 5.08eV, in reference [3] and [4], respectively [24].

In the 3.06 eV spectrum the 2LO mode intensity is ~0.002 from that of the F_{2g} mode. When measured at the excitation energy of 3.81 eV, it becomes more than three orders of magnitude higher. The very good correlation between the 2LO and the absorption coefficient demonstrates the resonant Raman scattering with the O*2p* - Ce*4f* electronic transition in CeO_2. Most importantly, the band at ~590 cm^{-1} also follows the absorption coefficient. This serves as a clear indication that this band is of LO origin, which similarly to the 2LO and 3-6LO modes (with the latter absent in the off-resonant spectra) is activated under resonance. Hence, below the resonant absorption onset the bands around 500- 600 cm^{-1} are exclusively attributed to a second-order BZ transition and above the resonant onset it is mostly attributed to the D_1 and to the LO modes.

In light of this analysis, in **Figure 3** we assign the defect spectrum in the range of 500-600 cm^{-1} under resonant (3.81 eV) and off-resonant (3.06 eV) conditions, for the undoped ceria pellet. The Raman spectrum at 3.06 eV is practically similar to that of 2.33 eV (Figure 1a) and contain exclusively second-order BZ edge bands. Under resonant conditions, two bands positioned at ~540 cm^{-1} and ~590 cm^{-1} emerge at the expected positions of the D_1 band and the first order LO phonon, respectively. Some of the symmetry assignments of the second-order BZ edge bands, which are denoted in Figure 3, differ from those of Weber et al [1] (see **Table S1** in the SI) as they are more consistent with the up-to-date phonon dispersion curves [25], calculated for single crystal ceria. The following discussion offers physical interpretation of the observed resonant enhancement of the 1 to 6LO set in the CeO_2 UV-Raman spectrum.

The formation of small polarons in reduced ceria is central in the understanding of its ionic conductivity and optical characterization [26-28]. These are formed when electrons, left behind in the O vacancy upon its formation, are “self-trapped” at Ce^{4+} sites and occupy the narrow Ce *4f* band.

As a result, adjacent atoms or ions are displaced inducing local lattice distortion around the Ce site while breaking the translational symmetry of the crystal. The combination of the electron localization and the local lattice distortion comprises the small polaron. The strength of electron-phonon interactions in the small polaronic system scales with the number of LO phonons which "surround" the slow-moving polarons in the lattice [29].

Polaron creation and dynamics may be strongly interlinked with optical transitions excited within the oxide. According to Moser et al. [30] polaron creation and motion may be activated in a thin layer below the surface by UV optical transitions. Tunable polaronic conduction in anatase TiO_2 was explored by creating oxygen vacancies under deep UV radiation, which provide an effective electron-doping mechanism [30]. In the angle resolved photo emission spectrum (ARPES) up to 3LO satellite bands were detected, attributed to the formation of polarons. As for the ceria-based materials, the respective local transition is suggested to be that of the resonant *O2p - Ce4f*.

In the framework of the polaron formation mechanism, optical transition probability was argued to be related to the distribution of the LO phonons [31]. Static displacement of the normal coordinates of the **k**~0 phonons may also be produced by localized excitations that couple strongly to the lattice through the Fröhlich electron-phonon interactions [32]. The appearance under resonance of up to fifth-order LO modes in YbS [33] and up to sixth-order LO modes in the small polaronic, Fluorite structure system of UO_2 [34] were discussed in relation to the above mechanistic schemes. In both cases, the concurrent resonant dependence of the 1LO and 2LO was demonstrated.

Following the discussion above, we argue that the up to the sixth -order resonant Raman LO mode "forbidden" scattering, as seen in Figure 1 and Figure S3 of the SI, is related with the fundamental polaronic nature of CeO_{2-y} (with oxygen vacancy fraction $y/2 < 0.01$ estimated in our pellet [20]). The resonant nature of the LO and 2LO modes, seen in Figure 2 and the exclusive emergence of third and higher-order LO modes beyond ~3.06 eV clearly point to the manifestation of Fröhlich-type interactions. By assigning a *complete* sequence up to the sixth- order LO overtones we set the ground for a valid physical insight of the resonant process.

After elucidating the nature of the ~590 cm^{-1} mode as the LO phonon, below, we discuss the propensity to detect the D_2 defect-related band. This band, detected under off- resonant conditions, was argued [3-5] to appear at the same spectral position under resonant conditions only

with different relative intensities, however, the data described in **Figure 4** suggest a different interpretation. Raman spectra were acquired under two excitation energies, in resonant (3.81 eV) and off-resonant (1.96 eV) conditions, from the same position on a thin (~1 μm) film of 4% Sm doped ceria. Moderately doped ceria was chosen since it provides minimal defect mode shift, mostly attributed to lattice parameter expansion, allowing for convenient comparison to defect mode positions to those discussed for undoped ceria. Since thin films have a relatively small grain size and thickness, grain boundary to bulk ratio is high, making the defect spectrum more easily resolved at low concentrations. According to the Lorentzian line shape analysis the D_1 local mode at ~549 cm^{-1}, is found at the same position under the two excitation energies. However, the second mode at ~600 cm^{-1}, attributed to D_2 under off-resonant conditions [1-6] is red shifted by ~8 cm^{-1} under resonance to the expected LO phonon position. Although we expect for some D_2 band spectral contribution, it is not distinguishable since the resonant LO phonon overshadows it. Consequently, quantitative explicit correlation between the off-resonant Raman spectral analysis of defected ceria with those conducted under resonant conditions that is based on the D_2 intensity is not feasible; the defect bands sensitivity of this region under UV resonant conditions as demonstrated in [3] has to be discussed in view of the dominant nature of the LO mode.

In the UV excitation range the penetration depth is calculated to be ~20 nm, different from the off-resonant cases (for which the penetration depth is equivalent to the ~1μm film thickness). Defects and oxygen vacancies may therefore expected to significantly contribute in the former, and it is reasonable to expect some enhancement of the D_1 band [5] intensity relative to that of the F_{2g} mode. However, it is important to note that the local D_1 mode may also be enhanced in a similar manner to other studies systems that include local vibrational modes (LVMs), like in heavily Si doped GaAs, where the Raman intensity of the LVM was found (concurrently with the LO mode) to be resonantly tuned, as the excitation energy approached that of the GaAs E_1 bandgap [35]. The absence of UV- resonant enhancement of the D_2 defect mode may be explained by the fact that not all the LVMs meet the preconditions that render their enhancement. Particularly noteworthy is that one significant difference between the D_1 and D_2 modes, that may lead to their different behavior, is that polarons were shown to strongly couple to oxygen vacancies in doped ceria.

3.2. Local *vs.* average phonon modes in UV- Raman of $Ce_{1-x}Do_xO_{2-x/2}$

We follow the resonant Raman spectra of Lu, Gd, Sm or La doped ceria ceramic pellets (a-d, respectively, **Figure 5**) at several doping fractions, in order to substantiate the observed deviation of *local* and *average* structures from X-ray diffraction and absorption measurements (See Figure S1 of the SI). Central peak positions of the F_{2g}, D_1, 1LO (which, as discussed above, may contain some minor contribution from the D_2 [3,5] defect mode), 2LO and 3LO Raman modes were determined by Lorentzian line fit analysis. Although the 4LO modes were also clearly detected for in Lu-doped (Figure S3 of the SI) and <10% of Gd-doped ceria, they are omitted here for consistency. Mode Raman frequencies as function of Do mol% are shown in the top panels and reveal the following trends: i. The F_{2g} mode shift qualitatively follows the trend of lattice expansion in Gd, Sm and La (See $\Delta a/a_0$ in the top horizontal axis) by shifting to lower wavenumbers (red shift), and lattice contraction of Lu, by shifting to higher wavenumbers (blue shift). It is therefore evident that other effects (like phonon anharmonicity), which play a significant role and therefore must be considered in any quantitative analysis of the F_{2g} mode frequency shift, do not overshadow the volume effects. The 1-3LO modes normalized frequencies generally follow the same trend for the F_{2g} mode for the two extreme cases of La and Lu but for Gd and Sm they show moderately opposite trend. Furthermore, the behavior of the D_1 local mode in the vicinity of V_O defects (the analysis of which is likely facilitated by UV resonant enhancement), shows also a similar trend to that of the 1-3LO behavior.

For La and Lu the general trend of the Do^{3+} mol% frequency dependence for the D_1 *local mode* is similar to that of the F_{2g} *phonon*, i.e. it adheres to the expansion/contraction in average structures. However, for Gd and Sm, the D_1 trend is opposite to the F_{2g} mode with the former representative of local lattice contraction around defects. This observation has several significant implications: *i.* The above evidence supports the trends suggested by X-ray diffraction and EXAFS for Lanthanide-doped ceria (Figure S1). As discussed in the introduction, a clear deviation in local and average structures (linked to the presence of local strain fields in the material) appears particularly for the intermediate size dopants Sm and Gd. These complementary X-ray and Raman scattering data suggest that for good ionic conductors/strongly anelastic ceria materials the presence of local strain is favorable. *ii.* The contraction observed in the first shell distances *Ce-O* and *Do-O*

by EXAFS is likely occurring in the vicinity of V_O defects (assigned experimentally to the D_1 mode).

Another important outcome of Figure 5 is that the nLO (n=1-3) modes, which appear under strong electron-phonon interactions, also show a general Do^{3+} mol% frequency dependence, similar to that of the D_1 mode. For La-doped ceria ω_{nLO}/n red shifts, similarly to the F_{2g} and D_1 modes, but for the Gd and Sm -doped ceria it shows a unique blue shift, opposing to the F_{2g} phonon %mol dependence. This remarkable result may suggest that the extent of electron- phonon interactions for the ω_{nLO} modes may be linked in Lanthanide-doped ceria to the excessive formation of local strains around the oxygen vacancy defect.

4 Conclusions

CeO_2 has a narrow, empty band of *Ce4f* states that lies between a *O2p* based valence band and a *Ce5d* based conduction band. The *O2p - Ce4f* optical band gap is positioned at ~3. 2 eV with an absorption band centered at ~3.8 eV. We investigated the Raman scattering of bulk CeO_2 in the excitation energy range of 1.96–3.81 eV. The resonant enhancement profile of the longitudinal optical LO phonon at ~590 cm^{-1}, closely follows that of the 2LO band and both track the optical absorption band profile of the O*2p* - Ce*4f* electronic transition. Assigning a *complete* sequential set up to the sixth- order LO overtones and the exclusive emergence of third and higher-order LO modes above 3.06 eV clearly points to the manifestation of Fröhlich-type interactions.

The ~600 cm^{-1} off-resonant D_2 band (denoted in the literature as MO_8-type complex ($M=Do^{3+}$)), is overshadowed, under resonant conditions, by the LO phonon scattering. Consequently, quantitative explicit correlation between the off-resonant Raman spectral analysis of doped-ceria with those conducted under resonant conditions, based on the D_2 intensity, is not feasible; the defect sensitivity of this region under resonant conditions [3] cannot be attributed exclusively to surface defect enrichment due to the short penetration depth of UV radiation, and has to be discussed in view of the dominant nature of the LO mode.

We applied the above mode assignment to study the UV-resonant Raman spectra of Lu, Gd, Sm or La doped ceria ceramic pellets. For La and Lu the general trend of the Do^{3+} *mol*% frequency dependence for the D_1 *local mode* is similar to that of the F_{2g} phonon, i.e. it qualitatively follows the expansion/contraction in average structures. However, for Gd and Sm, opposite trends are

observed in the *local* D_1 and average F_{2g} modes (contraction *vs.* expansion, respectively). The observed trends complement earlier findings for the above dopants, where EXAFS derived Do-O and Ce-O interatomic distances were found to contract while an average expansion is observed in the lattice parameter using XRD (Figure S1). The contraction in Ce-O and Do-O distances may be closely linked to formation of V_O complexes, which are represented by the D_1 *local* Raman mode. In addition, deviation of trends in *local* and *average* structures was recently linked to the presence of local strain fields, responsible for anelastic effects in doped ceria. The clear deviation in these trends observed here for Gd and Sm ceria solutions, which are known to exhibit maximum ionic conductivity, may therefore suggest that local strain is preferable for their performance.

The 1-3LO modes also show general trend which is similar to the D_1 mode. This remarkable result suggests that the extent of electron- phonon interactions for the ω_{nLO} modes may be linked to the excessive formation of local strains around the oxygen vacancy defect in Lanthanide-doped ceria.

*Corresponding author: *T.Livneh@nrcn.gov.il*

Supporting Information. Comparison of cation-oxygen distances derived from X-ray diffraction (average structure) to X-ray absorption spectroscopy (local structure). 4% Sm doped ceria thin film deposition and X-ray diffraction. Full range UV- Raman spectrum of undoped CeO_2. Updated assignments of the second- order Raman in CeO_2, based on recent up-to-date calculation of phonon dispersion curves.

5 Acknowledgments

This work was supported by the PAZY foundation grant #2018/57. This work was also supported in part by the BioWings project, which has received funding from the European Union's Horizon 2020 under the Future and Emerging Technologies (FET) program with a grant agreement No. 801267. This research is made possible in part by the historic generosity of the Harold Perlman Family. We gratefully acknowledge Prof. Juan C. Nino for making available the Sm-doped ceria pellets and Dr. Michael Aizenstein for making available the La-doped ceria pellets. We also gratefully acknowledge Dr. Ariel Ismach for enabling us to measure the Raman spectrum of ceria under the 405 nm laser excitation.

6 Figures

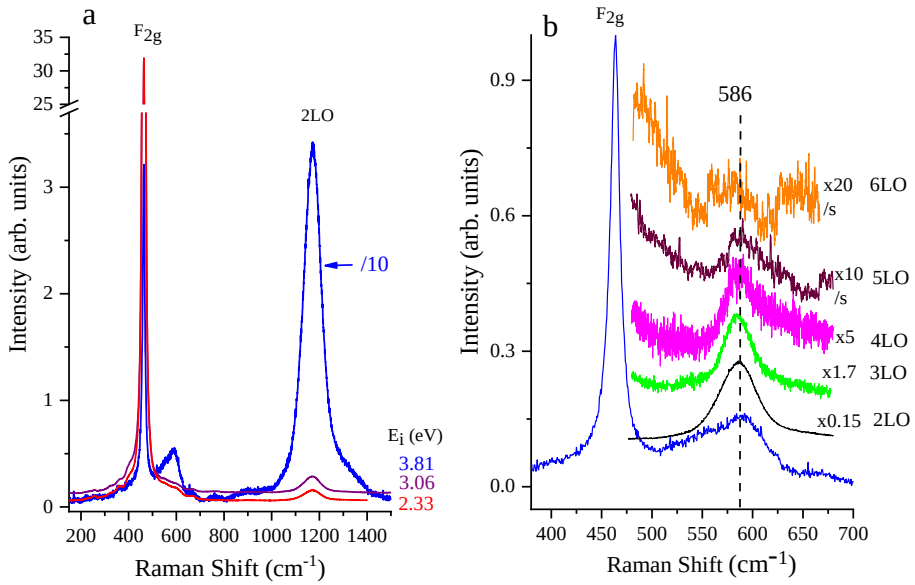

Figure 1: a) Raman spectra of an undoped CeO_2 pellet, measured at the excitation energy of 2.33 eV - 3.81 eV. b) the appearance of up to sixth-order LO modes is demonstrated for the 3.81 eV spectrum by "slicing" the spectrum into segments that are shifted by $-n\cdot\omega_{LO}$ with ω_{LO}=586 cm^{-1}. The intensity magnification of each "slice" is denoted and /s stands for smoothed spectrum. The full "unsliced" spectrum is shown in Figure S3 of the supporting information.

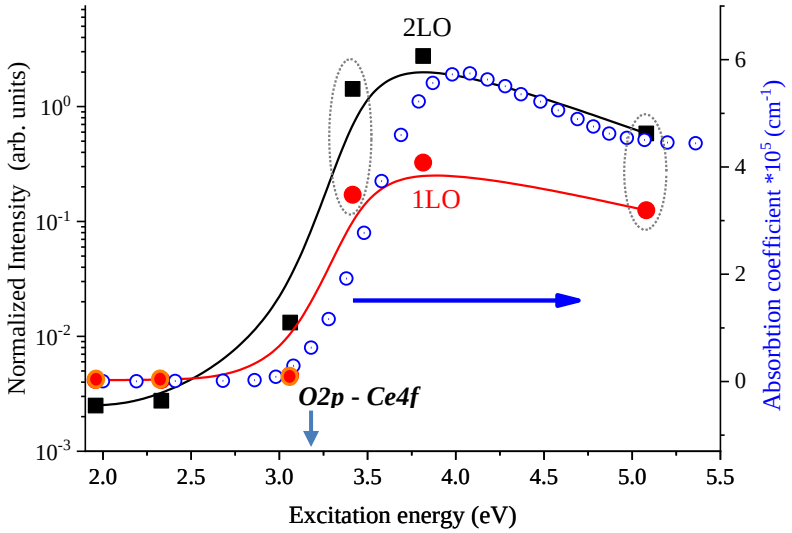

Figure 2: Intensities (normalized to that of the F_{2g} mode) of the 2LO (black squares) and ~590 cm^{-1} (red circles) bands extracted from the spectra in Fig.1. The value at 3.41 eV is estimated from a spectrum of CeO_2 nano-powders in reference [3] and the value at 5.08 eV is estimated from the spectrum of nano-octahedral crystals of ceria in reference [4] (see note (24)). The normalized intensities are compared to excitation energy dependence of the absorption coefficient, α (empty circles), is derived from the extinction coefficient, ε_2, of bulk CeO_2 [8] according to $\alpha=4\pi\varepsilon_2/\lambda$ (λ- the wavelength). Below the resonant absorption onset (~3.2 eV) the bands around ~590 cm^{-1}, which are denoted with additional orange outer empty circles, are attributed to second-order BZ transitions with no contribution from the 1LO mode-see Figure 3.

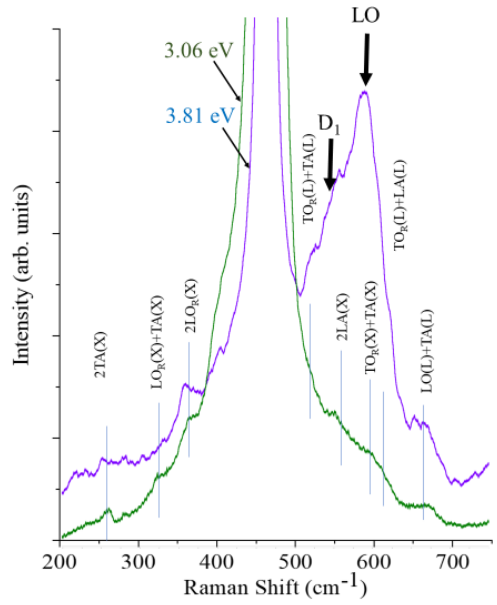

Figure 3: Raman spectra taken at the excitation energies of 3.06 eV and 3.81 eV. Assignment of second-order BZ edge transitions appear in both spectra (and discussed in the supporting information- see Table S1) are denoted. The ~540 cm^{-1} and ~590 cm^{-1} bands emerge under resonance (3.81 eV) at the expected positions of the D_1 band and the LO modes, respectively.

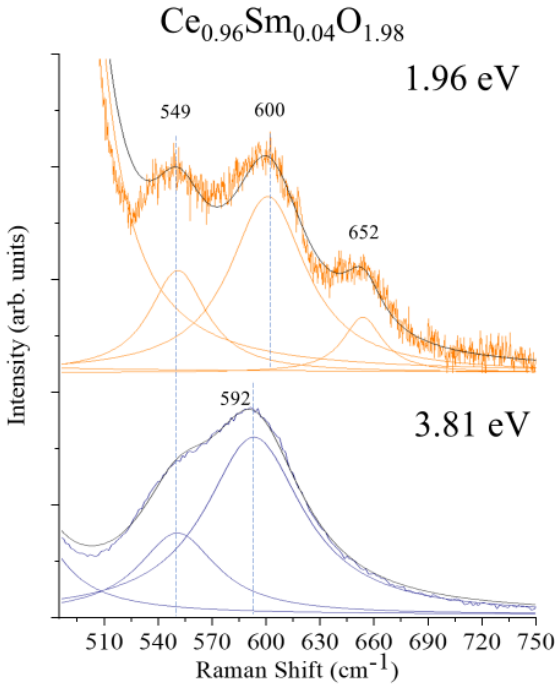

Figure 4: Raman spectra collected from 4% Sm doped ceria thin films at off-resonant 1.96 eV (up) and resonant 3.81 eV (bottom) excitation energies, both normalized to the F_{2g} peak intensities.

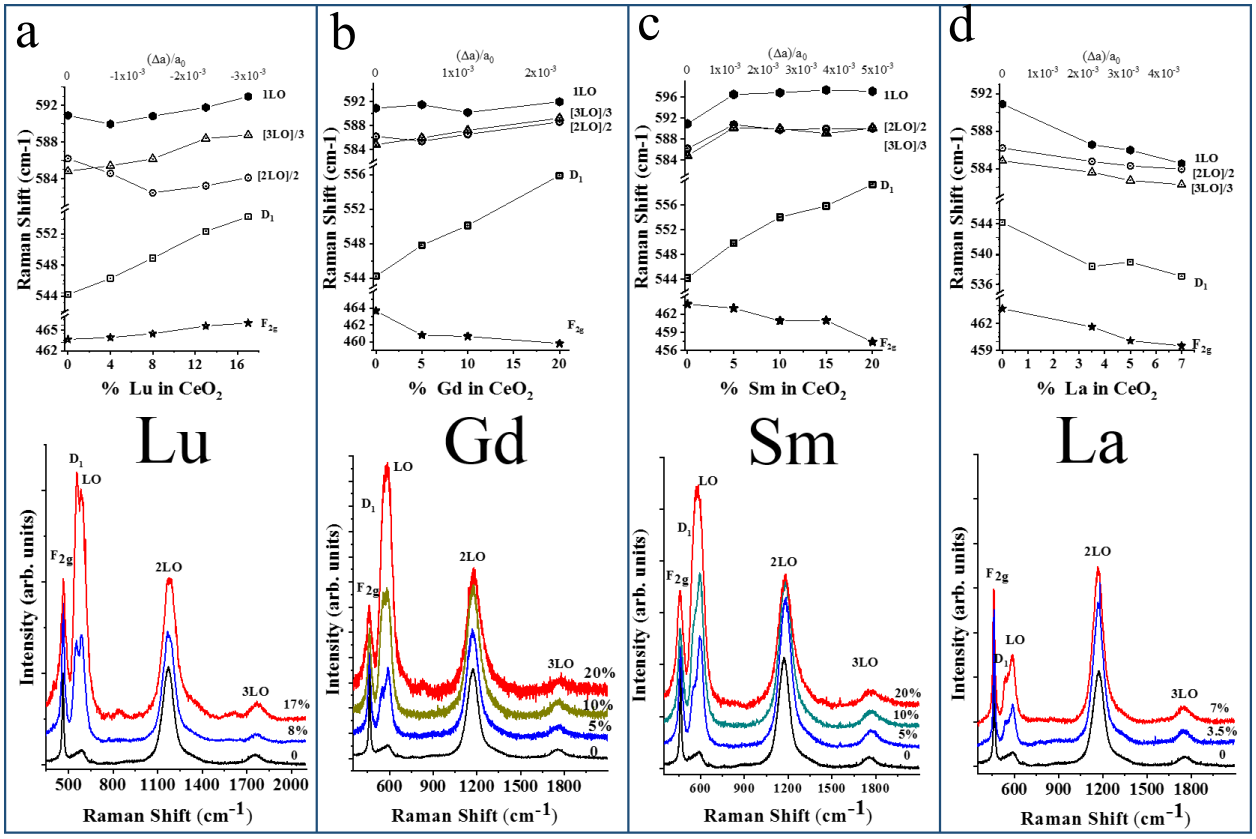

Figure 5: a-d) bottom panels: UV-resonant Raman spectra of Lu, Gd, Sm and La- doped ceria ceramic pellets, at the denoted doping fractions in mol% of Ln^{3+} ions. Upper panels: Lorentzian line fit of mode Raman peak frequencies as function of Do^{3+} *mol*%. The lattice expansion ($\Delta a/a_0$), presented in the top horizontal axis is based on the modified lattice constants, as extracted from XRD measurements.

7 References

1. Weber, W.; Hass, K.; McBride, J. Raman study of CeO_2: second-order scattering, lattice dynamics, and particle-size effects. *Phys. Rev. B* **1993,** 48, (1), 178-185.
2. Nakajima, A.; Yoshihara, A.; Ishigame, M. Defect-induced Raman spectra in doped CeO_2. *Phys. Rev. B* **1994,** 50, (18), 13297-13307.
3. Taniguchi, T.; Watanabe, T.; Sugiyama, N.; Subramani, A.; Wagata, H.; Matsushita, N.; Yoshimura, M. Identifying defects in ceria-based nanocrystals by UV resonance Raman spectroscopy. *J. Phys. Chem. C* **2009,** 113, (46), 19789-19793.
4. Wu, Z.; Li, M.; Howe, J.; Meyer III, H. M.; Overbury, S. H. Probing defect sites on CeO_2 nanocrystals with well-defined surface planes by Raman spectroscopy and O_2 adsorption. *Langmuir* **2010,** 26, (21), 16595-16606.
5. Li, L.; Chen, F.; Lu, J.-Q.; Luo, M.-F. Study of defect sites in $Ce_{1-x}M_xO_{2-\delta}$ (x= 0.2) solid solutions using Raman spectroscopy. *J. Phy. Chem. A* **2011,** 115, (27), 7972-7977.

6. Artini, C.; Pani, M.; Carnasciali, M. M.; Buscaglia, M. T.; Plaisier, J. R.; Costa, G. A. Structural features of Sm-and Gd-doped ceria studied by synchrotron X-ray diffraction and μ-Raman spectroscopy. *Inorg. Chem.* **2015,** 54, (8), 4126-4137.
7. Schilling, C.; Hofmann, A.; Hess, C.; Ganduglia-Pirovano, M. V. Raman spectra of polycrystalline CeO2: A density functional theory study. *J. Phys. Chem. C* **2017,** 121, (38), 20834-20849.
8. Goubin, F.; Rocquefelte, X.; Whangbo, M.-H.; Montardi, Y.; Brec, R.; Jobic, S. Experimental and theoretical characterization of the optical properties of CeO_2, $SrCeO_3$, and Sr_2CeO_4 containing Ce^{4+} (f^0) ions. *Chem. Mater.* **2004,** 16, (4), 662-669.
9. Mochizuki, S., Radiative optical modes of vibration in CeO_2 thin films. *phys. Status Solidi B* **1985,** 128, (1), 23-30.
10. Kraynis, O.; Timoshenko, J.; Huang, J.; Singh, H.; Wachtel, E.; Frenkel, A. I.; Lubomirsky, I. Modeling strain distribution at the atomic level in doped ceria films with extended X-ray absorption fine structure spectroscopy. *Inorg. Chem.* **2019,** 58 11, 7527-7536.
11. Giannici, F.; Gregori, G.; Aliotta, C.; Longo, A.; Maier, J.; Martorana, A. Structure and oxide ion conductivity: local order, defect interactions and grain boundary effects in acceptor-doped ceria. *Chem. Mater.* **2014,** 26, (20), 5994-6006.
12. Kossoy, A.; Wang, Q.; Korobko, R.; Grover, V.; Feldman, Y.; Wachtel, E.; Tyagi, A. K.; Frenkel, A. I.; Lubomirsky, I. Evolution of the local structure at the phase transition in CeO_2-Gd_2O_3 solid solutions. *Phys. Rev. B* **2013,** 87, (5), 054101.
13. Koettgen, J.; Martin, M. Coordination numbers in Sm-Doped ceria using X-ray absorption spectroscopy. *J. Phys. Chem. C* **2019**, 123 (11), 6333–6339
14. Scavini, M.; Coduri, M.; Allieta, M.; Brunelli, M.; Ferrero, C. Probing complex disorder in $Ce_{1-x}Gd_x O_{2-x/2}$ using the pair distribution function analysis. *Chem. Mater.* **2012,** 24, (7), 1338-1345.
15. Coduri, M.; Masala, P.; Allieta, M.; Peral, I.; Brunelli, M.; Biffi, C. A.; Scavini, M. Phase transformations in the CeO_2–Sm_2O_3 system: A multiscale powder diffraction investigation. *Inorg. Chem.* **2017,** 57, (2), 879-891.
16. Koettgen, J.; Grieshammer, S.; Hein, P.; Grope, B. O. H.; Nakayama, M.; Martin, M. Understanding the ionic conductivity maximum in doped ceria: trapping and blocking. *Phys. Chem. Chem. Phys.* **2018,** 20, (21), 14291-14321.
17. Wachtel, E.; Frenkel, A. I.; Lubomirsky, I. Anelastic and electromechanical properties of doped and reduced ceria. *Adv. Mater.* **2018**, 1707455.
18. Yavo, N.; Nissenbaum, A.; Wachtel, E.; Shaul, T. E.; Mendelson, O.; Kimmel, G.; Kim, S.; Lubomirsky, I.; Yeheskel, O. Rapid sintering protocol produces dense ceria-based ceramics. *J. Am. Ceram. Soc.* **2018,** 101, (11), 4968-4975.
19. Yavo, N.; Noiman, D.; Wachtel, E.; Kim, S.; Feldman, Y.; Lubomirsky, I.; Yeheskel, O. Elastic moduli of pure and gadolinium doped ceria revisited: Sound velocity measurements. *Scr. Mater.* **2016,** 123, 86-89.
20. Varenik, M.; Zhang, X.-D.; Leitus, G.; Yavo, N.; Carmieli, R.; Wachtel, E.; Guo, X.; Lubomirsky, I. Van Vleck paramagnetism in undoped and Lu-doped bulk ceria. *Phys. Chem. Chem. Phys.* **2018,** 20, (42), 27019-27024.
21. Varenik, M.; Cohen, S.; Wachtel, E.; Frenkel, A. I.; Nino, J. C.; Lubomirsky, I. Oxygen vacancy ordering and viscoelastic mechanical properties of doped ceria ceramics. *Scr. Mater.* **2019,** 163, 19-23.
22. Li, L.; Nino, J. C. Ionic conductivity across the disorder–order phase transition in the $SmO_{1.5}$– CeO_2 system. *J. Eur. Ceram. Soc.* **2012,** 32, (13), 3543-3550.
23. Chen, W.; Navrotsky, A. Thermochemical study of trivalent-doped ceria systems: CeO_2–$MO_{1.5}$ (M= La, Gd, and Y). *J. Mater. Res.* **2006,** 21, (12), 3242-3251.
24. Both are characterized with 80-90 nm grain sizes (see ref. 3 and Fig. S2 of ref. 4), for which the $2LO/F_{2g}$ intensity ratio is not expected to significantly differ from that found for our pellet measured under

similar excitation energies; According to Fig. 7 of Ref. 1 the increase in the width due to deviation from single crystal is expected not to exceed ~0.5 cm^{-1}.
25. Buckeridge, J.; Scanlon, D.; Walsh, A.; Catlow, C.; Sokol, A. Dynamical response and instability in ceria under lattice expansion. *Phys. Rev. B* **2013,** 87, (21), 214304.
26. Sun, L.; Huang, X.; Wang, L.; Janotti, A. Disentangling the role of small polarons and oxygen vacancies in CeO_2. *Phys. Rev. B* **2017,** 95, (24), 245101.
27. Shoko, E.; Smith, M.; McKenzie, R. H. Charge distribution and transport properties in reduced ceria phases: a review. *J. Phys. Chem. Solids* **2011,** 72, (12), 1482-1494.
28. Tuller, H.; Nowick, A. Small polaron electron transport in reduced CeO_2 single crystals. *J. Phys. Chem. Solids* **1977,** 38, (8), 859-867.
29. Kittel, C., *Introduction to solid state physics*. Wiley New York: 1996.
30. Moser, S.; Moreschini, L.; Jaćimović, J.; Barišić, O.; Berger, H.; Magrez, A.; Chang, Y.; Kim, K.; Bostwick, A.; Rotenberg, E. Tunable polaronic conduction in anatase TiO_2. *Phys. Rev. Lett.* **2013,** 110, (19), 196403.
31. Ruello, P.; Becker, K.; Ullrich, K.; Desgranges, L.; Petot, C.; Petot-Ervas, G. Thermal variation of the optical absorption of UO_2: determination of the small polaron self-energy. *J. Nuc. Mater.* **2004,** 328, (1), 46-54.
32. Cardona, M.; Güntherodt, G., *Light scattering in solids II: basic concepts and instrumentation*. Springer-Verlag: 1982.
33. Merlin, R.; Güntherodt, G.; Humphreys, R.; Cardona, M.; Suryanarayanan, R.; Holtzberg, F. Multiphonon processes in YbS. *Phys. Rev. B* **1978,** 17, (12), 4951-4958.
34. Livneh, T.; Sterer, E., Effect of pressure on the resonant multiphonon Raman scattering in UO_2. *Phys. Rev. B* **2006,** 73, (8), 085118.
35. Ramsteiner, M.; Wagner, J.; Ennen, H.; Maier, M., Resonance Raman scattering of Si local vibrational modes in GaAs. *Phys. Rev. B* **1988,** 38, (15), 10669-10676.

TOC Graphic